Journal of ELECTRONIC MATERIALS, Vol. 39, No. 12, 2010
DOI: 10.1007/s11664-010-1353-7

Formation and Growth of Intermetallic Compound Cu_6Sn_5 at Early Stages in Lead-Free Soldering

M.S. PARK[1] and R. ARROYAVE[1,2,3]

1.—Department of Mechanical Engineering, Texas A&M University, College Station, TX 77843, USA. 2.—Materials Science and Engineering Program, Texas A&M University, College Station, TX 77843, USA. 3.—e-mail: rarroyave@tamu.edu

In this work, the early stages of the formation and growth of the intermetallic compound Cu_6Sn_5 during soldering reactions between a Cu substrate and liquid Sn are examined through phase-field simulations. The liquid Sn-based solder (L phase) and the copper substrate (α phase) are considered to be under metastable equilibrium conditions that eventually lead to nucleation of the Cu_6Sn_5 intermetallic compound (IMC) (η phase) at the solid/liquid interface. Nucleation is incorporated into the model through a classical treatment considering that individual nucleation events follow a Poisson distribution function. The driving forces for the nucleation and phase transformations are obtained by coupling the phase-field simulations to CALPHAD models. In the phase-field simulations, physical properties such as liquid surface as well as IMC interfacial energies are treated parametrically to probe the behavior of the system under various growth conditions. The simulations are compared with previous works and are shown to have good (qualitative) agreement with recent detailed studies on the early stages of the interaction between Cu and liquid Sn.

Key words: Multiphase field model, morphology, lead-free soldering, intermetallic compound growth, Cu_6Sn_5, nucleation

INTRODUCTION

Fundamental understanding of the formation and growth of intermetallic compounds (IMC) during lead-free soldering is considerably important in electronic materials packaging, since the nature and morphology of the resulting interfaces greatly affect the reliability of the soldered joints.[1–3] From synthesis to actual operation, the interfaces formed at solder joints undergo multiple morphological changes as the substrate/solder reaction progresses. Among these various stages of evolution, incipient formation of IMCs at the soldering interfaces is one of the most important phenomena that eventually control the sequence and morphology of later IMC layer growth.

Over the past decade, many researchers have investigated the nature of the interaction between liquid Sn and solid Cu substrates during soldering reactions.[4–18] These works suggest that, upon contact, Cu and liquid Sn react to form two distinct IMCs [Cu_6Sn_5 (η phase) and Cu_3Sn (ε phase)], which precipitate at different stages of the soldering reaction. Most research seems to suggest that, at the very early stages of the soldering reaction, the η phase precipitates first. Lee et al.[19] compared the driving forces for the precipitation of the two different Cu-Sn phases at the *metastable* solid Cu/liquid Sn interface. Under these local metastable equilibrium conditions, the η phase has the largest driving force for precipitation. If one assumes that other contributions (e.g., interfacial energies) to the activation barrier for nucleation are comparable between the two phases, the larger thermodynamic driving force would explain the observed precipitation sequence.[19] After the precipitation of the η phase, the precipitation of the ε phase at the η/Cu substrate interface becomes thermodynamically possible, and it is thus usually observed at later stages of the soldering reactions.[19]

(Received February 25, 2010; accepted August 2, 2010; published online September 10, 2010)

Earlier works have focused on experimental characterization of the late stages of growth and coalescence of η and ε phases during lead-free soldering reactions between Sn and Cu.[4–18] More recently, several groups have investigated the formation of the η phase at the early stages of soldering reactions.[20–23] These latter works have found that individual Cu_6Sn_5 grains seem to appear at random positions along the (metastable) solid/liquid interface within a few milliseconds. After the η grains appear, they have been found to spread along the interface without much growth perpendicular to the solder/substrate interface until they meet with other spreading grains, forming a relatively uniform IMC layer of Cu_6Sn_5. After the initial formation of the IMC layer, its thickness increases at the expense of the underlying substrate, with individual grains acquiring a scallop-like morphology[18] that continues to grow perpendicularly to the interface.

While there has been considerable experimental effort aimed at understanding the morphological evolution of IMC layers during soldering reactions, research on computer simulation of IMC formation and growth has been rather limited. IMC growth has been modeled previously[24–26] by using phase-field approaches.[27,28] These mathematical models have proved to be a very useful tool to investigate the microstructural evolution of IMCs as a function of factors such as solid/liquid interfacial energies, grain boundary energies, relative mass transport enhancement by grain boundaries, and so forth.[24–26] So far, these simulation efforts have focused on the evolution of IMC layers at late stages.

To model the formation and early-stage evolution of IMCs, nucleation must be incorporated into the simulations. In the past, different approaches to incorporate nucleation into phase-field models have been proposed. Introducing Gaussian noise into the phase-field evolution equations can induce nucleation of a thermodynamically allowable state, provided that the fluctuations necessary for growth of stable nuclei of the new phase can be accessed within the simulation time. A strategy to avoid this limitation has been proposed by Simmon and coworkers.[29–31] This approach is based on assuming that nucleation events are essentially stochastic processes which can be modeled through a Poisson distribution. The parameters for the classical nucleation theory formulation are defined in terms of kinetic and thermodynamic properties of the system in question.

In this study, we will briefly introduce a nucleation model for the formation of the η phase along a Cu/Sn interface which was derived from previous nucleation models developed within the context of phase-field modeling of solidification phenomena.[29–31] The proposed nucleation model will be incorporated into a multiphase field model derived from previous works[26–28] for the evolution of grains of Cu_6Sn_5 under different conditions. We will show different morphologies of IMC grains and layers during lead-free soldering as a function of material parameters. In this work, we will assume that the Cu_6Sn_5 phases are the only ones to precipitate, limiting this investigation to the early stages of the soldering reaction. The rate of growth of the individual IMC grains will be controlled by the diffusion rates, while the coarsening of the IMC grains as well as the nucleation kinetics will be controlled by using different solder/IMC interface energies.

NUCLEATION MODELING

The incorporation of realistic models for nucleation of a new phase still constitutes a significant problem in phase-field modeling. The most common approach consists of adding Gaussian noise to the dynamic equations. This approach requires that the necessary local perturbations of the system configuration are small enough that they can be sampled within the normal running time of the simulation.[32] An alternative method for incorporating nucleation into phase-field simulations relies on explicitly incorporating nuclei throughout the simulation time by relying on classical nucleation theory.[29–31,33,34] The probability for nucleation of a new phase at a random location in space and time is determined, and nuclei are "seeded" accordingly. Once a nucleus forms, it occupies a definite volume of space, which in turn yields a zero event probability for formation of additional nuclei within the same volume.[29,30,32] The stochastic nucleation process can thus be approximated by a Poisson distribution:

$$P_n = 1 - \exp[-(J \cdot v \cdot \Delta t)], \tag{1}$$

where Δt is the time interval considered, v represents the volume of a nucleus, and the nucleation rate J can be obtained from a classical nucleation model. In this work, we adopt the model used to simulate nucleation in an undercooled liquid developed in Ref. 30

$$J = J_0 \exp\left[-\frac{16\pi\sigma_{sl}^3}{3kT(\Delta G_V)^2}\left(\frac{\cos^3\theta - 3\cos\theta + 2}{4}\right)\right], \tag{2}$$

where J_0 is a frequency factor with order of magnitude $10^{39\pm1}$ (m^{-3} s^{-1}) in volume nucleation and $10^{31\pm1}$ (m^{-2} s^{-1}) for surface nucleation. σ_{sl} represents the energy of a solid/liquid interface. k is Boltzmann's constant. θ is the contact angle of a nucleus with respect to the solid substrate. ΔG_V is the driving force between the crystal (η phase) and the melt.

The preferential nucleation of Cu_6Sn_5 over Cu_3Sn can be explained by examining the free energy diagram shown in Fig. 1. At t = 0, the substrate (α) and the liquid (L) solder exist in a state of metastable equilibrium. When the common tangent construction is applied to this metastable equilibrium, the free energy of the Cu_6Sn_5 η phase lies below this line. The thermodynamic driving

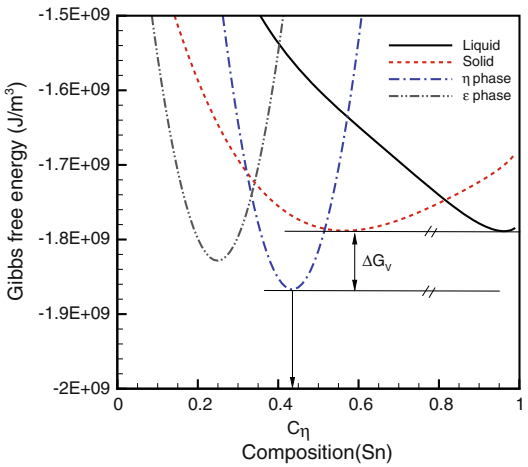

Fig. 1. Gibbs free energy of individual phases (S, L, and η) with respect to composition at 523 K. Driving force can be obtained from the free energy profiles.

force ΔG_V for nucleation of this phase corresponds to the difference between the free energy of this phase and the chemical potentials of the system components corresponding to the metastable α/L equilibrium. This driving force is positive, meaning that the formation of the η phase at the solid/liquid metastable interface is thermodynamically possible. On the other hand, while the ε phase (Cu_3Sn) also has a positive driving force for nucleation, the magnitude of this driving force is smaller, and the expected nucleation rate for this phase during early stages would be much smaller than for the η phase.[19] This seems to be corroborated by experimental observations.

The driving force for nucleation of the η phase is indicated schematically in Fig. 1. The free energies of individual phases can be obtained from the CALPHAD model of Shim et al.[35] (see Appendix). Calculation of the driving force requires determination of the common tangent connecting the free energy curves of the α and L phases. It should be mentioned that, in this work, the local metastable equilibrium at any point where the α and L phases coexist is calculated at every time step of the simulation.

MULTIPHASE FIELD AND DIFFUSION EQUATIONS

The simulated system initially consists of a Sn-based liquid solder (L) and a Cu solid substrate (α). In this work, each individual η grain is assigned its own phase-field variable, according to the multiphase field formalism.[26–28,32] The spatial distribution of the liquid solder, the substrate, and the nucleated grains in the system is mathematically expressed by using N arrays of phase fields $\phi_i(x, t)$ (i = 1, …, N), which can be expressed with multiphase field variables. The phase-field variables in this model can be defined as ϕ_1 for the solid substrate, $\phi_{2,\ \ldots,\ N-1}$ for the nucleating grains, and ϕ_N for the liquid solder. Each of these nonconserved field variables represents occupation of a given point in the computational domain by the solid substrate, the liquid solder, and/or any of $N-2$ individual grains of the η phase.

The free energy density f of the multiphase system can be defined as follows:[27,36]

$$f = \sum_{j>i}\sum_{i}\left[-\frac{\varepsilon_{ij}^2}{2}\nabla\phi_i\cdot\nabla\phi_j + \omega_{ij}\phi_i\phi_j\right] + \sum_i \phi_i f^i(c_i), \tag{3}$$

where f^i is the chemical free energy density of the ith phase, which depends on the phase composition c_i. ε_{ij} is the gradient energy coefficient, which is related to the energy penalty involved in forming an interface, and ω_{ij} is a double-well potential representing the energy barrier between two phases i and j. Initially, the composition of the different coexisting phases is assumed to correspond to the bulk compositions. We then determine the compositions of coexisting phases at any given point of the computational domain by establishing the chemical potential equilibrium condition,[36] which has the advantage that it somewhat relaxes the maximum interfacial thickness allowable in the numerical implementation of phase-field simulations and avoids the formation of extraneous secondary "energy barriers" resulting from discontinuities in the chemical potentials across an interface.[36]

Within the phase-field formalism, the evolution equations are obtained from variational principles[26–28,32]:

The phase-field kinetic equation is given by:

$$\frac{\partial\phi_i}{\partial t} = -\frac{2}{N_p}\sum_{i\neq j}\chi_i\chi_j M_{ij}\left[\frac{\partial F}{\partial\phi_i} - \frac{\partial F}{\partial\phi_j}\right], \tag{4}$$

where

$$\frac{\partial F}{\partial\phi_i} = \sum_{i\neq j}\left[\frac{\varepsilon_{ij}^2}{2}\nabla^2\phi_j + \omega_{ij}\phi_j\right] + f^i(c_i) - f_c c_i, \tag{5}$$

and the diffusion equation is

$$\frac{\partial c}{\partial t} = \nabla\cdot\left(D(\phi_i)\sum_{i=1}^{N}\phi_i\nabla c_i\right). \tag{6}$$

Constraints for the multiphase field and diffusion equations are, respectively,

$$\sum_{i=1}^{N}\phi_i = 1, \tag{7}$$

and

$$c(x,t) = \sum_{i=1}^{N}\phi_i c_i. \tag{8}$$

χ_i (in Eq. 4) is equal to 1 when the corresponding phase exists in that region of the computational domain and equal to 0 when the corresponding phase field is absent, and N_p represents the number of coexisting phases at a calculated position: $N_p(x, t) = \sum_i^N \chi_i(x, t)$. The multiphase field equation is only valid on the phase interfaces, since the presence of only one phase at any point of the calculation domain renders χ_i or χ_j equal to 0. M_{ij} represents the mobility of the interfacial region.

Model parameters for the multiphase field equation can be obtained from a stationary solution of the phase-field equation along a planar interface, which results in two relationships between model parameters and material parameters associated with the definition of the interface energy as a function of gradient energy coefficient and phase field with a referred interface width[25,28]:

$$\varepsilon_{ij} = \frac{4\sqrt{\xi\sigma_{ij}}}{\pi} \quad \text{and} \quad \omega_{ij} = \frac{2\sigma_{ij}}{\xi}, \tag{9}$$

where ξ is half of the width of the interface, and σ_{ij} is the interface energy for the corresponding phases.

Numerical Implementation

A Cu-Sn binary system will be considered. The system is initially composed of a Sn-rich liquid solder (L) and a Cu-rich solid substrate (α). Meanwhile, IMC grains of Cu_6Sn_5 (η) are randomly seeded based on the nucleation methodology discussed above. The phase-field equation and diffusion equation are numerically computed by using the finite-difference method for the spatial domain and Euler scheme for the temporal domain in two dimensions. The mesh size for the calculation domain is fixed as $\Delta x = 1.0 \times 10^{-7}$ (m) and the half-width of the interface, ξ, is set to $4\Delta x$.

The nucleation probability P_n is calculated according to the material parameters at each time step and every four nodal points in the interface. Meanwhile, a random number is generated. If the generated number is smaller than the average P_n from every four nodal points, the nodes will be transformed to a single nucleus. Because the nodes are transformed, the composition of the surrounding subdomains must change to enforce mass conservation. The amount of residual solute after the phase transformation can be added exclusively to the neighboring liquid nodes, since diffusion rates in the liquid are much higher than through the solid phases. To ensure smooth compositional gradients at the nuclei/matrix interface, the steady-state diffusion equation is solved after each of the nuclei is introduced. If P_n does not satisfy the criterion described above, no nucleus is transformed, and the calculation will be continued at the next interface position to be satisfied with the nucleation probability. It is noted that a newborn nucleus is not allowed to overlap with other nuclei in the simulation.

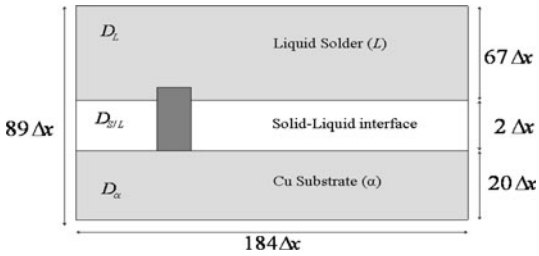

Fig. 2. A schematic configuration for the computational domain. The system is $184\Delta x \times 89\Delta x$. Cu substrate and liquid solder are positioned between 0 and $20\Delta x$ and between $22\Delta x$ and $89\Delta x$. The position between $20\Delta x$ and $22\Delta x$ is set to be the α/L interface. Nuclei (shown as a rectangular in the interface) will be randomly positioned at the interface based on the Poisson distribution function.

The size of the nucleus is determined by the critical radius of the nucleus from the classical nucleation theory.[20] For the size of a nucleus we use the radius of the critical nucleus $r_{cri} = (2\sigma_{L\eta}\sin(\theta)/\Delta G_V)$ of a classical nucleation theory.[20] This roughly corresponds to a size of $4\Delta x \times 4\Delta x$ in our simulations.

Figure 2 shows a schematic illustration of the computational domain and the position of the nuclei as it appears at the interface. The size of the system is set to be $184\Delta x \times 89\Delta x$. The Cu substrate and liquid solder are positioned between 0 and $20\Delta x$ and between $22\Delta x$ and $89\Delta x$, respectively. The position between $20\Delta x$ and $22\Delta x$ is set to be the α/L interface. Periodic boundary conditions are applied to the sides of the calculation domain, and Neumann boundary conditions are applied to the top and bottom of the calculation domain for ϕ_i and c. The calculations are finished when $t = 10$ s.

The free energy densities per unit molar volume of individual phases can be obtained from the CALPHAD method[35] (see Appendix) with molar volume $v_m = 16.29$ (cm^3/mole). The equilibrium phase compositions can be used as $c_L^{\alpha L} = 0.977$ and $c_\alpha^{\alpha L} = 0.1957$, and the equilibrium composition of the η phase can be calculated by using free energy equations as shown in the previous section ($c_\eta = 0.435$), where $c_\alpha^{\alpha L}$ is the equilibrium composition of the α phase at the α/L interface, and the other terms are defined correspondingly. The initial compositions of the Cu substrate and liquid solder are set to be $c_\alpha = 0.002$ and $c_L = c_L^{\alpha L}$.

Simulation parameters, such as interfacial energies and mobilities, are notoriously hard to obtain from experimental results. They are thus used as simulation parameters which are fitted to experimental data. The diffusivities and other material parameters employed in the numerical calculation are summarized in Table I, which also includes the effective nucleation parameters obtained by Gagliano et al.[20] for two different substrate surface roughness conditions (obtained by polishing the substrate to two different surface finishes of 1 μm and 6 μm).

Table I. Material parameter values for use in simulating the formation and growth of IMC layer during lead-free soldering

$D_L = 3.96 \times 10^{-9} e^{-33.02/RT}$ (m^2/s)[37], $D_\eta = 1.28 \times 10^{-11} e^{-53.92/RT}$ (m^2/s)[38]
$D_\alpha = 2.95 \times 10^{-5} e^{-138.84/RT}$ (m^2/s)[37], $D_{\eta L} = 2.0 \times 10^{-1} D_L$ (m^2/s)
$D_{\eta\alpha} = 2.0 \times 10^{-3} D_L$ (m^2/s), $D_{GB} = 2.0 \times 10^{3} D_\eta$ (m^2/s)
$\sigma_{\eta L} = 0.055$ (J/m^2)[20], $\sigma_{\eta\alpha} = \sigma_{GB} = 0.3$ (J/m^2)[25]
$M_{\eta L} = 1.0 \times 10^{6} D_L$ (m^2/s), $M_{\eta\alpha} = M_{GB} = 7.0 \times 10^{4} D_L$ (m^2/s)
$J_0 = 1.08 \times 10^{29}$ (m^2/s), $\theta = 22.7$ for 1 μm surface roughness
$J_0 = 2.11 \times 10^{29}$ (m^2/s), $\theta = 23.1$ for 6 μm surface roughness

RESULTS AND DISCUSSION

The morphologies of IMC (Cu_6Sn_5) grain growth, including nucleation behavior, will be modeled using the temperature-dependent diffusion coefficients and thermodynamic driving force for precipitation of the η nuclei as well as different nucleation parameters obtained empirically by Gagliano et al.[20] Simulations are carried out at four different temperatures, which provide different diffusion coefficients as well as driving forces for precipitation of η nuclei. Because of the difficulty of determining D_{GB}, this quantity is considered to be a model parameter whose values are set to be relative to the bulk diffusion coefficient within Cu_6Sn_5 (η) grains. The fast diffusion through the grain boundaries, rather than through η grains, can be simulated by using $D_{GB} = 2.0 \times 10^3 D_\eta$, and the low diffusion through the grain boundaries can be considered by using $D_{GB} = D_\eta$. For all cases, the initial solder composition is set to $c_L = c_L^{L\eta}$,[25] and the L/η interfacial energy is set to be $\sigma_{\eta L} = 0.055$ J/m^2,[20] as shown in Table I.

Figure 3 shows the morphology of the IMC grains with 1 μm surface roughness (see corresponding nucleation parameters in Table I) with T = (a) 240°C, (b) 260°C, (c) 280°C, and (d) 300°C at t = 1 s. IMC grains randomly nucleate in space and time according to Poisson statistics. The number of nuclei at early stages depends on the soldering conditions. At each of the simulation temperatures, η grains developed scallop-like morphologies at t = 1 s for all cases, filling the whole Cu/Sn interface.[20] This effect is more pronounced for higher simulation temperatures.

The number of nuclei for each case is different due to the stochastic nature of the nucleation process, which is in turn strongly dominated by the system temperature. At low temperatures, nucleation rates are much higher, resulting in complete coverage of the substrate at very short times (Fig. 3a and b).[21] In the case of higher simulation temperatures (Fig. 3c and d), fewer nuclei are nucleated due to lower nucleation driving forces, and the nuclei are likely to grow in width rather than in height. This behavior can be explained as follows: Forming the Cu_6Sn_5 phase requires Cu and Sn. During the vertical growth of Cu_6Sn_5, Cu should be supplied from the Cu substrate to the η/L interface. However, because of the longer diffusion distance, this process takes a longer time. On the other hand, Cu supply at the triple junction likely occurs easily, because the components necessary to make Cu_6Sn_5 are close

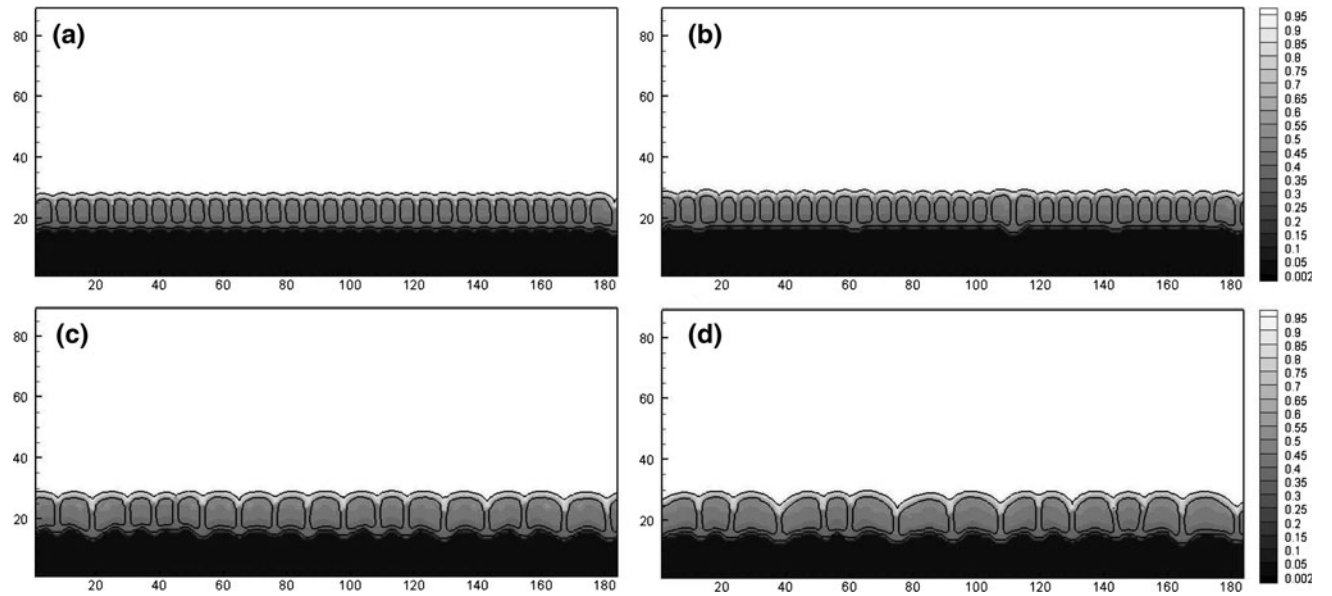

Fig. 3. Morphology of IMC layer during lead-free soldering with nucleation effect (1 μm surface roughness) at 1 s, where T = (a) 240°C, (b) 260°C, (c) 280°C, and (d) 300°C.

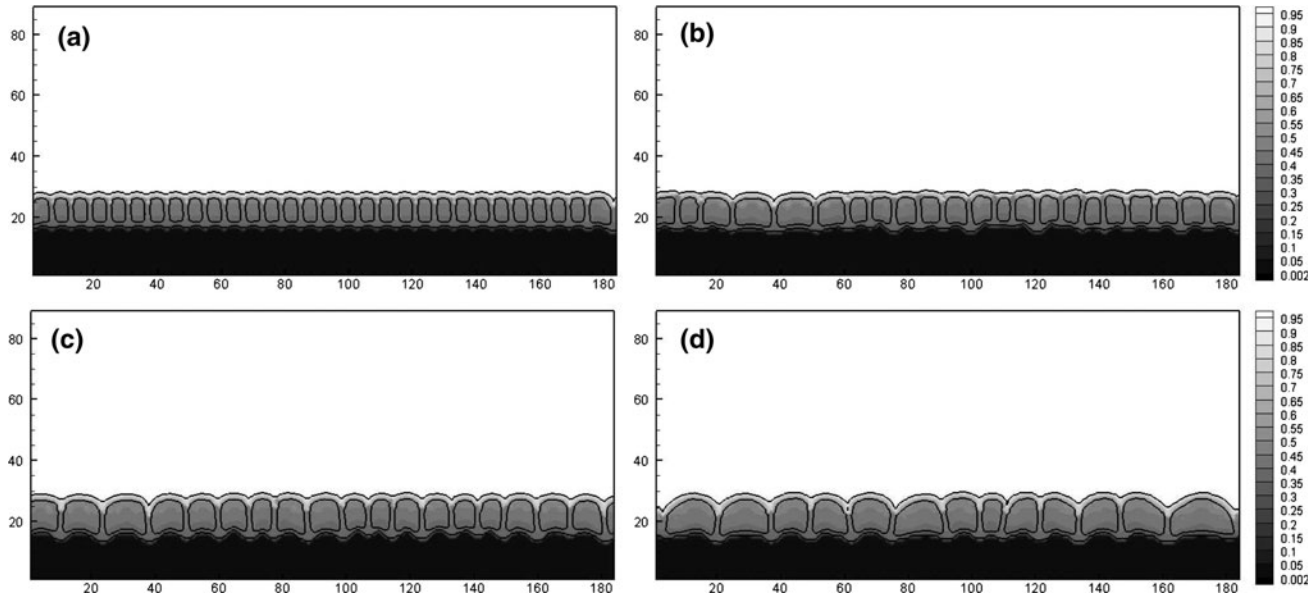

Fig. 4. Morphology of IMC layer during lead-free soldering with nucleation effect (6 μm surface roughness) in 1 s, when T = (a) 240°C, (b) 260°C, (c) 280°C, and (d) 300°C.

together, so that forming Cu_6Sn_5 at the edge of the grain occurs faster than forming Cu_6Sn_5 at the top of the grains.

Figure 4 shows nucleation of the IMC grains with 6 μm surface roughness (see corresponding nucleation parameters in Table I) with T = (a) 240°C, (b) 260°C, (c) 280°C, and (d) 300°C at t = 1 s. The difference in surface roughness will not affect the morphology change of IMC grain growth, but will change the nucleation rate due to the fact that different surface roughness results in different areas and consequently different densities of potential heterogeneous nucleation sites.[20] Nuclei that form in the case of 6 μm surface roughness appear to be similar to those that form in the case of 1 μm surface roughness in terms of shape and distribution based on simple visual comparison.

Figure 5 shows the evolution of (a) Cu substrate thickness, (b) η IMC layer thickness, and (c) the number of grains with respect to different surface roughness (1 μm roughness and 6 μm roughness) until t = 10 s. Cases 1 and 2 show the results with fast grain boundary diffusion [$D_{GB} = 2.0 \times 10^3 D_\eta$ (m^2/s)] and low grain boundary diffusion [$D_{GB} = D_\eta$ (m^2/s)], respectively. In the consideration of different D_{GB}, the number of nuclei at the initial time appears to be the same, but different growth of nuclei appears after a few seconds. Contrary to the early stages of morphological evolution, one can find that η grain growth in the late stages for case 1 and case 2 are similar to the results from previous works.[10,18,25] In the low-D_{GB} scenario (case 2), the Cu substrate is not readily dissolved to form Cu_6Sn_5 grains, so that the thickness of the IMC phase shows a lower rate of increase compared with case 1, which is in good agreement with previous work.[25]

At the early stage ($t < 0.1$ s) during lead-free soldering in Fig. 4, the Cu substrate thickness remains unchanged, the thickness of the IMC increases gradually, and the number of IMC grains is not changed. The Cu substrate thickness decreases slowly, because the microstructure evolution is dominated by nucleation rather than growth. During these early stages, IMC grains grow horizontally rather than vertically (with respect to the solid/liquid interface). Microstructure coarsening (growth of large grains at the expense of smaller ones and the corresponding decrease in number of grains) will not occur until the grains impinging on one another. Upon full coverage of the Cu substrate, Cu thickness reduction starts to accelerate at the same time that the thickness of the IMC layer increases. The number of IMC grains decreases (IMC microstructure coarsening) only at the later stages of the soldering reaction. This is consistent with the experimental observations by Lord and Umantsev[21] and Gorlich and Schmitza.[18]

At later stages of the soldering reaction the grain boundaries are grooved, and partial penetration (wetting) of the η grain boundaries is observed. The flat η/L interface becomes initially rounded, and microstructure coarsening starts. The degree of microstructure coarsening depends on the grain boundary diffusion coefficient. With a fast grain boundary diffusion coefficient, we can expect that the large flux of Cu and Sn is delivered through the grain boundary, resulting in the fast vertical IMC layer growth as well as microstructure coarsening. This is represented by case 1 in Figs. 4 and 5. On the other hand, if the grain boundary diffusion coefficient is smaller (case 2), less supply of Cu and Sn leads to a smaller rate of decrease of

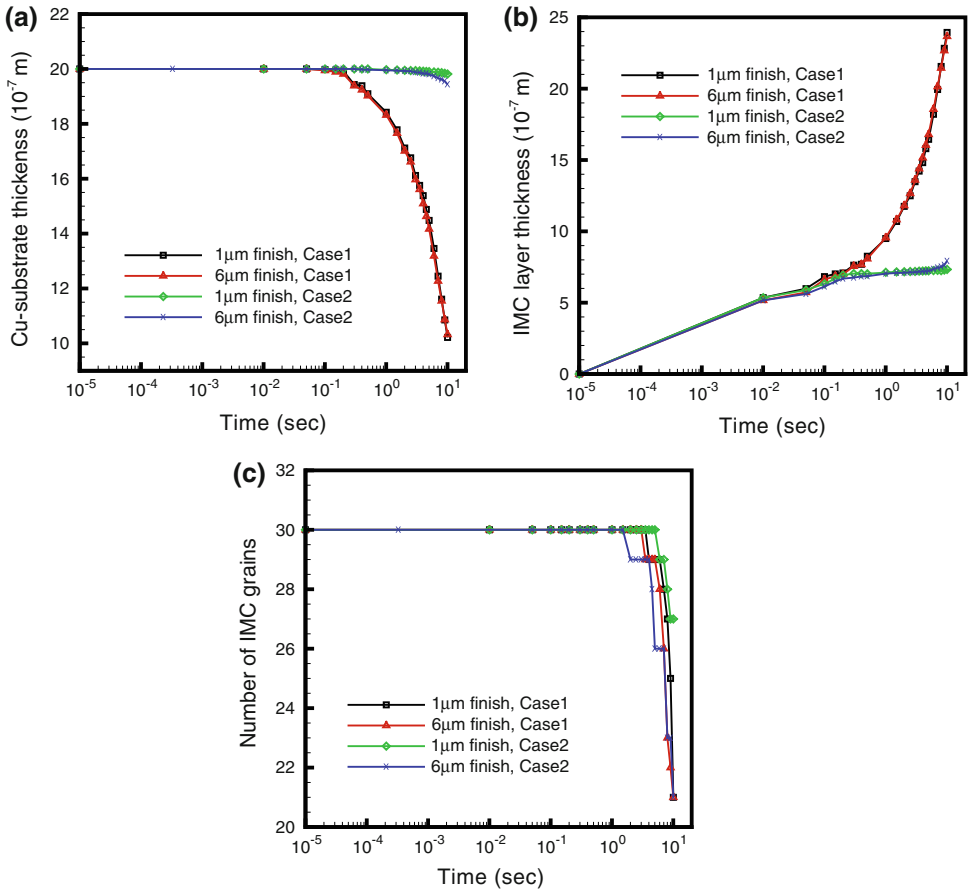

Fig. 5. (a) Evolution of Cu substrate, (b) η IMC layer thickness, and (c) the number of grains with respect to different surface roughness (1 μm roughness and 6 μm roughness) until t = 10 s. Case 1 and case 2 show the results with fast grain boundary diffusion [$D_{GB} = 2.0 \times 10^3 D_\eta$ (m^2/s)] and low grain boundary diffusion [$D_{GB} = D_\eta$ (m^2/s)], respectively. (Color online).

Cu substrate thickness as well as a smaller increase of the IMC layer thickness.

Although different surface roughness conditions apparently do not influence the shape and distribution of IMC grains during the early stages of the soldering reaction, more detailed investigation actually shows that different nucleation conditions lead to observable differences in the number of IMC grains as well as their average size, as shown in Fig. 6. The figures present the number of IMC grains per μm^2 (Fig. 6a and b) and the average radius of IMC grains (Fig. 6c and d) with respect to 240°C ≤ T ≤ 300°C compared with experimental results.[20] Due to uncertainty of D_{GB}, fast grain boundary diffusion (case 1) is used in Fig. 6a and c, while low grain boundary diffusion (case 2) is applied in Fig. 6b and d.

In agreement with experimental observations,[20] it is found that the number of η grains per unit area increases with an increase in the reaction temperature, until a maximum is reached between 260°C and 270°C. At higher temperatures, the number of grains decreases. This maximum occurs due to the optimal combination of the thermodynamic driving force for IMC nucleation as well as kinetics for IMC growth. This phenomenon implies that the average radius of η grains is dependent not only on the growth kinetics of η grains but also on nucleation rate, due to the fact that lower reaction temperatures lead to higher stochastic nucleation and earlier grain coalescence. Because of the large number of η grains between T = 260°C and T = 270°C, the minimum radius is found within this temperature range, as shown in Fig. 6c and d, reflecting the results for the number of particles per unit area shown in Fig. 6a and b. From Fig. 6, it is also found that the fast-D_{GB} (case 1) simulations result in a larger number of IMC grains when compared with experiments, while the low-D_{GB} (case 2) simulations result in a smaller number of IMC grains across the temperature range examined. Case 1, however, seems to agree better with experiments, suggesting that grain boundary diffusion during Cu/Sn soldering is considerably faster than bulk diffusion across IMC grains.

The computational investigation of Cu_6Sn_5 nucleation and growth during lead-free soldering is somewhat more complicated than previous simulations in which nucleation was not considered. However, this effort allowed us to introduce a more

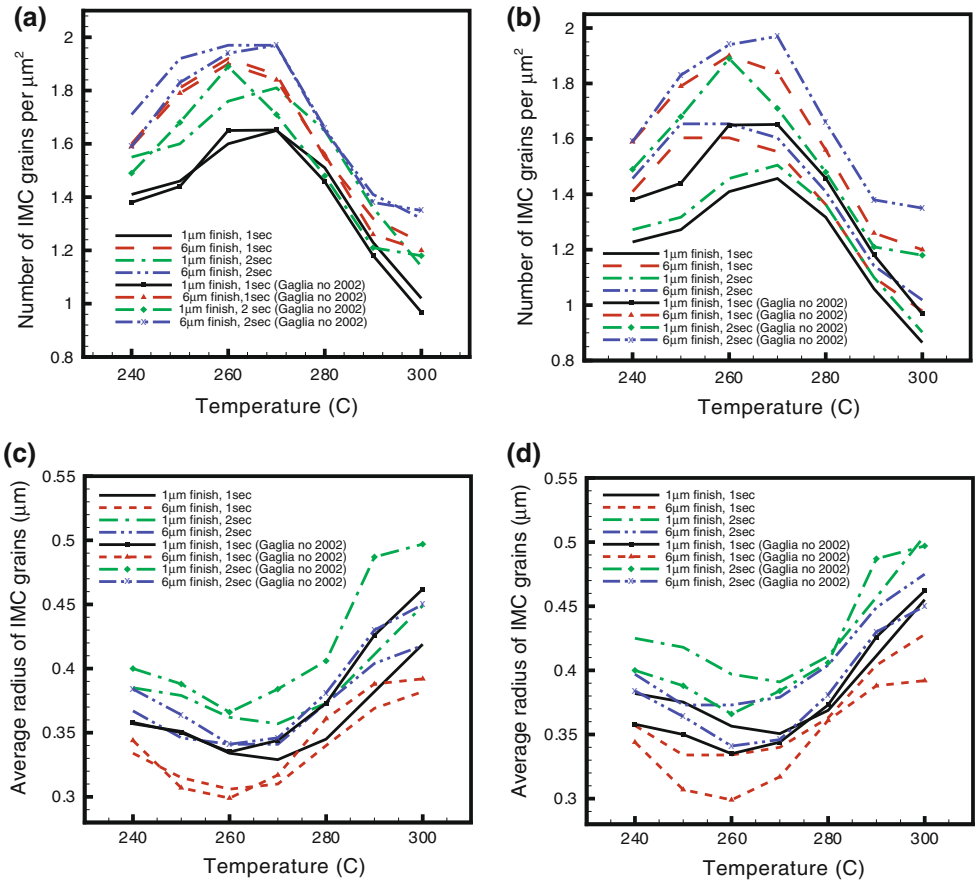

Fig. 6. Comparison of the present and experimental results[20] for (a, b) number of IMC layer per μm^2 and (c, d) average radius of a IMC grain with respect to $240 \leq T \leq 300$. Fast grain boundary diffusion [$D_{GB} = 2.0 \times 10^{-2} D_L$ (m^2/s)] and low grain boundary diffusion [$D_{GB} = 2.0 \times 10^{-4} D_L$ (m^2/s)] are applied in (a, c) and (b, d), respectively. (Color online).

realistic physical description of the soldering system. This work shows that it is now possible to qualitatively reproduce many previous experimental results on the nucleation behavior at early stages of soldering, lateral growth of IMC grains prior to microstructure coarsening, as well as the evolution of a scallop-like morphology of the IMC layer once the substrate/solder interface is completely covered with Cu_6Sn_5.

CONCLUSIONS

This study examines the nucleation behavior of Cu_6Sn_5 IMCs during the reaction of liquid Sn on Cu substrate in early stages of a soldering system with a phase-field model with CALPHAD thermodynamic descriptions and a nucleation model. The phase-field model with the explicit nucleation model allows the determination of different material characteristics that change the morphology of IMC grains formed at the early stages in the Cu/Sn soldering. Nucleation of Cu_6Sn_5 IMC grains during lead-free soldering was performed by using a nucleation model that considers nucleation events through a Poisson distribution function, and the morphological formation and growth of the IMC (Cu_6Sn_5) grains after the nucleation stage were performed using a multiphase field model. The simulations were performed by using two different grain boundary diffusion coefficients in η IMC grains.

The present results agree well with experiments in which different temperatures and surface roughness (which changes the number of available sites for heterogeneous nucleation) were used to explore the nucleation behavior in the soldering system.[20] They can be summarized as follows: (1) Cu_6Sn_5 formed at early stages in all cases, which is in good agreement with experimental research,[20] and Cu_6Sn_5 predominantly grew in a horizontal direction until the η grains impinge on one another. (2) After grains impinged, the scallop shape of the grains can be observed, which results from grain coarsening.[21,25] (3) Although the formation and growth of the IMC grains were observed to be somewhat different from in the research by Huh et al.[25] during early stages, the behavior of the IMC grains (or layer) applied with different material parameters (e.g., D_{GB}) at the late stages eventually appears similar to in the research by Huh et al.[25] (4) Although the differences seem slight, the number of η grains per unit area increases with increase

of reaction temperature until between 260°C and 270°C, and then decreased afterward regardless of nucleation conditions, which is in good agreement with experimental results.[20] Finally, comparison between simulations and experiments[20] suggests that the actual grain boundary diffusion coefficient in η grains is at least two orders of magnitude higher than the diffusion coefficient in bulk η grains.

ACKNOWLEDGEMENTS

Most of the calculations were carried out on the CAT cluster of the department of Chemical Engineering at Texas A&M university. This research was supported by the National Science Foundation under NSF Grant Nos. CMMI-0758298 and CMMI-1027689.

APPENDIX

Free energies of individual phases that can be obtained from the CALPHAD model by:[35]

$$\begin{aligned} G_\alpha &= (1-c)G^\alpha_{\mathrm{Cu}} + cG^\alpha_{\mathrm{Sn}} \\ &\quad + RT[(1-c)\ln(1-c) + c\ln c] \\ &\quad + c(1-c)\left[L^\alpha_0 + L^\alpha_1(1-2c)\right], \\ G_\eta &= 2.0\times 10^5(c-0.435)^2 + 0.545G^\alpha_{\mathrm{Cu}} + 0.455G^{\mathrm{SER}}_{\mathrm{Sn}} \\ &\quad - 6869.5 - 0.1589T, \\ G_{\mathrm{L}} &= (1-c)G^{\mathrm{L}}_{\mathrm{Cu}} + cG^{\mathrm{L}}_{\mathrm{Sn}} \\ &\quad + RT[(1-c)\ln(1-c) + c\ln c] \\ &\quad + c(1-c)\left[L^{\mathrm{L}}_0 + L^{\mathrm{L}}_1(1-2c) + L^{\mathrm{L}}_2(1-4c-4c^2)\right], \end{aligned}$$

where

$$\begin{aligned} &G^\alpha_{\mathrm{Cu}} = -19073.0, \quad G^\alpha_{\mathrm{Sn}} = -27280.0, \\ &G^{\mathrm{SER}}_{\mathrm{Sn}} = 346160.0, \quad G^{\mathrm{L}}_{\mathrm{Cu}} = -11083.0, \\ &G^{\mathrm{L}}_{\mathrm{Sn}} = -28963.0, \\ &L^\alpha_0 = -11448.0, \quad L^\alpha_1 = -11694.0, \\ &L^{\mathrm{L}}_0 = -10487.0, \quad L^{\mathrm{L}}_1 = -18198.0, \\ &L^{\mathrm{L}}_2 = 10528.4. \end{aligned}$$

REFERENCES

1. M. Abtew and G. Selvaduray, *Mater. Sci. Eng. R.* 27, 95 (2000).
2. K.N. Tu and K. Zeng, *Mater. Sci. Eng. R.* 27, 1 (2001).
3. T. Laurila, V. Vuorinen, and J.K. Kivilahti, *Mater. Sci. Eng. R.* 49, 1 (2005).
4. Z. Mei, A.J. Sunwoo, and J.W. Morris Jr., *Metall. Trans. A* 23A, 857 (1992).
5. Y. Wu, J.A. Sees, C. Pouraghabagher, L.A. Foster, J.L. Marshall, E.G. Jacobs, and R.F. Pinizzotto, *J. Electron. Mater.* 22, 769 (1993).
6. D.R. Frear and P.T. Vianco, *Metall. Mater. Trans. A* 25A, 1509 (1994).
7. S. Bader, W. Gust, and H. Hieber, *Acta Metall. Mater.* 43, 329 (1995).
8. H.K. Kim and K.N. Tu, *Appl. Phys. Lett.* 67, 2002 (1995).
9. H.K. Kim and K.N. Tu, *Phys. Rev. B* 53, 16027 (1996).
10. S.K. Kang, R.S. Rai, and S.J. Purushothaman, *Electron. Mater.* 25, 1113 (1997).
11. Y.G. Lee and J.G. Duh, *J. Mater. Sci.* 33, 5567 (1998).
12. M. Schaefer, R.A. Fournelle, and J.J. Liang, *Electron. Mater.* 27, 1167 (1998).
13. C.H. Zhong and S. Yi, *Solder. Surf. Mount Technol.* 11, 44 (1999).
14. W.K. Choi and H.M. Lee, *J. Electron. Mater.* 29, 1207 (2000).
15. C.K. Shin, Y.J. Baik, and J.Y. Huh, *J. Electron. Mater.* 30, 1323 (2001).
16. P.L. Tu, Y.C. Chan, K.C. Hung, and J.K.L. Lai, *Scripta Mater.* 44, 317 (2001).
17. K.S. Kim, S.H. Huh, and K. Suganuma, *J. Alloys Compd.* 352, 226 (2003).
18. J. Gorlich and G. Schmitza, *Appl. Phys. Lett.* 86, 053106 (2005).
19. B.J. Lee, N.M. Hwang, and H.M. Lee, *Acta Mater.* 45, 1867 (1997).
20. R.A. Gagliano, G. Ghosh, and M.E. Fine, *J. Electron. Mater.* 31, 1195 (2002).
21. R.A. Lord and A. Umantsev, *J. Appl. Phys.* 98, 063525 (2005).
22. C. Pan, C. Yu, and K. Lin, *Appl. Phys. Lett.* 93, 061912 (2008).
23. J. Gong, C. Liu, P. Conway, and V. Silberschmodt, *Acta Mater.* 56, 4291 (2008).
24. M. Ode, T. Koyama, H. Onodera, and T. Suzuki, *J. Electron. Mater.* 32, 1534 (2003).
25. J.Y. Huh, K.K. Hong, Y.B. Kim, and K.T. Kim, *J. Electron. Mater.* 33, 1161 (2004).
26. M.S. Park and R. Arroyave, *J. Electron. Mater.* 38, 2525 (2009).
27. I. Steinbach and F. Pezzolla, *Physica D* 134, 385 (1999).
28. S.G. Kim, W.T. Kim, T. Suzuki, and M. Ode, *J. Cryst. Growth* 261, 135 (2004).
29. J.P. Simmon, C. Shen, and Y. Wang, *Scripta Mater.* 43, 935 (2000).
30. J.P. Simmon, Y. Wen, C. Shen, and Y.Z. Wang, *Mater. Sci. Eng. A* 365, 136 (2004).
31. J. Li, J. Wang, and G. Yang, *J. Cryst. Growth* 309, 65 (2007).
32. J.A. Warren, T. Pusztai, L. Környei, and L. Gránásy, *Phys. Rev. B* 79, 014204 (2009).
33. Y.H. Wen, J.P. Simmon, C. Shen, C. Woodward, and Y. Wang, *Acta Mater.* 51, 1123 (2003).
34. J.D. Robson, *Acta Mater.* 52, 4669 (2004).
35. J.H. Shim, C.S. Oh, B.J. Lee, and D.N. Lee, *Z. Metallkd.* 87, 205 (1996).
36. S.G. Kim, W.T. Kim, and T. Suzuki, *Phys. Rev. E* 60, 7186 (1999).
37. H. Mehrer, *Diffusion in Solids* (Berlin: Springer, 2007).
38. M. Onishi and H. Fujibushi, *Trans. JIM.* 16, 539 (1975).